First-principles theory of infrared absorption spectra at surfaces and interfaces: Application to the Si(100):H_2O surface

Feliciano Giustino
Department of Physics, University of California at Berkeley, California 94720, USA and Materials Sciences Division, Lawrence Berkeley National Laboratory, Berkeley, California 94720, USA

Alfredo Pasquarello
Institute of Theoretical Physics and Institut Romand de Recherche Numérique en Physique des Matériaux (IRRMA), Ecole Polytechnique Fédérale de Lausanne (EPFL), CH-1015 Lausanne, Switzerland

(Received 30 March 2008; published 6 August 2008)

We calculate the transverse and the longitudinal infrared absorption spectra of the hydrated silicon surface using a first-principles approach. The absorption spectra are computed for two different configurations of water molecules dissociatively chemisorbed on the Si(100)-(2×1) surface at full coverage. Our calculations compare favorably with the experimental spectra for both the frequency and the intensity of the absorption peaks. Our results suggest the possibility of combining infrared spectroscopy and first-principles theoretical modeling to investigate the phase diagram of the Si(100):H_2O surface and similar systems. We also provide a detailed discussion of the underlying formalism, already introduced by Giustino and Pasquarello [Phys. Rev. Lett. **95**, 187402 (2005)]. The methods described here are of general validity and provide a basis for the theoretical modeling of infrared spectroscopy at surfaces and interfaces.

DOI: 10.1103/PhysRevB.78.075307 PACS number(s): 78.30.−j

I. INTRODUCTION

Recent years have witnessed a rapidly growing interest in the chemical functionalization of semiconductor surfaces, including those of silicon, germanium, and silicon carbide, both from the experimental and the theoretical standpoints.[1–3] Of particular importance for its ubiquity in electronic and photovoltaic devices is the Si(100) surface. The interface of silicon with its native oxide layer can be obtained through a wet-oxidation process, where the oxygen is supplied to the clean silicon surface through water vapor. In this area, elucidating the atomic-scale mechanisms of the interaction between water and the Si(100) surface would help defining rational approaches to interfacial growth at the nanoscale. The behavior of water on Si is also of relevance in the study of the optical properties of Si nanostructures in presence of water for applications in photonics and sensing technology.[4]

Infrared (IR) spectroscopy constitutes a nondestructive analytical tool to probe in real time the structural, vibrational, and dynamical properties of thin films with an atomic-scale resolution. The development of high-resolution surface infrared spectroscopy has allowed the study of hydrated silicon surfaces at submonolayer coverage.[5] In order to interpret the experimental spectra it is common practice to resort to quantum-chemical calculations which provide the vibrational frequencies of model clusters in realistic surface configurations.[6–8] Although this combination of experiment and theory has proven very successful so far, calculations based on cluster models of the surface still present significant limitations. Vibrational frequencies are often rescaled empirically and absorption intensities are not provided in a systematic way. Furthermore, a procedure for calculating the longitudinal component of the *p*-polarized spectra has so far not been proposed in the literature.

In this work we present first-principles calculations of the longitudinal optical (LO) and transverse-optical (TO) IR absorption spectra of the Si(100):H_2O surface. The calculations are based on the theory of the IR absorption at surfaces and interfaces introduced in Ref. 9. The absorption is here obtained in terms of microscopic dynamical properties of the surface and the substrate, namely, the vibrational frequencies of the substrate and the adsorbates, the Born and Callen dynamical charges, and the high-frequency and the static dielectric permittivities of the combined system. Our calculations compare favorably with the high-resolution IR data in Ref. 10 for both the energy and the intensity of the absorption peaks.

The paper is organized as follows. In Sec. II we describe the theoretical framework for the calculation of the IR absorption spectra. We present the general theory for both the total and the local (layer-resolved) absorption spectra, and we discuss the formulas used in the practical calculations. In Sec. III we present our results for the hydrated Si surface at full coverage in two different structural configurations, and we compare our results with experiment. In Sec. IV we summarize our findings and discuss possible future directions. We reserved Appendixes A and B for establishing the connection between the present theory of IR absorption and the theory of the local permittivity at surfaces and interfaces presented in Ref. 11 and for providing a formal justification of the concept of local permittivity introduced heuristically in the same work.

II. THEORETICAL FRAMEWORK

A. LO and TO modes in thin films

The frequencies of the long-wavelength transverse and longitudinal vibrations of a polarizable medium correspond

to the poles and to the nodes of the long-wavelength dielectric function, respectively. In an extended solid, this property directly derives from the *in medium* Maxwell's equations[12] and from the fact that a zone-center phonon with a TO (LO) frequency carries by definition a polarization field which is perpendicular (parallel) to the phonon wave vector $\mathbf{q}$.[13]

In the case of a thin film the previous relation looses its validity because Maxwell's equations must be supplied with appropriate boundary conditions at the surface of the film. However, we can still define the TO and LO modes using the poles and the nodes of the dielectric function as for an extended system. In this case, the boundary conditions at the surface of the film require that the polarization field associated to the vibrational excitations is either perpendicular (TO) or parallel (LO) to the normal direction of the film.[14,15]

Based on these considerations, it can be shown that the absorption coefficients for a thin film can be expressed in terms of two key quantities, which we denote as the transverse (I_t) and the longitudinal (I_ℓ) IR absorption functions,[9]

$$I_t(\omega) = \frac{\omega d}{c}\mathrm{Im}[\varepsilon(\omega)], \tag{1}$$

$$I_\ell(\omega) = \frac{\omega d}{c}\mathrm{Im}[-1/\varepsilon(\omega)]. \tag{2}$$

The quantity $\varepsilon(\omega)$ appearing in Eq. (1) is the dielectric-response function of the film (tensor indices are omitted for clarity), c is the speed of light, d is the thickness of the film, and ω is the frequency of the incident electromagnetic field. As an example, in the case of a suspended film, the absorption coefficients for incoming radiation with s or p polarization read

$$A_s(\omega) = I_t(\omega)/\cos\,\theta, \tag{3}$$

$$A_p(\omega) = [\cos^2\,\theta I_t(\omega) + \sin^2\,\theta I_\ell(\omega)]/\cos\,\theta, \tag{4}$$

where the prefactors do not depend on the frequency of the electromagnetic field. In more realistic situations, the scattering geometry and the optical effect of the substrate only affect the prefactors of I_t and I_ℓ and the way I_t and I_ℓ are combined in the expressions for the absorption intensities corresponding to s- or p-polarized light.[5,14,15] As a consequence, the IR absorption spectra of a thin film can be obtained by calculating the transverse and the longitudinal IR absorption functions of the film.

The theoretical framework described so far neglects retardation effects associated with the finite value of the speed of light. The explicit inclusion of retardation effects in the formalism, leading to the phonon-polariton dispersions, should have minor effects on the results. In fact, in the limit of very thin film the polariton frequencies coincide with the TO and LO frequencies of the corresponding extended solid.[16] This limit certainly applies to the case of surface adsorbates where typical thicknesses and wave numbers are $d \sim 1$ nm and $q \sim 1000$ cm^{-1}, respectively, resulting in a negligible phase shift of $qd \sim 10^{-4}$ throughout the film.

B. Total absorption spectra

In order to calculate the transverse and the longitudinal IR absorption functions [Eqs. (1) and (2)] from first principles, we find it convenient to adopt the dielectric functions ε_t^r and ε_ℓ^r which describe the response to the *external* electric fields rather than the macroscopic self-consistent fields (the superscript stands for "radiation"),[17]

$$\varepsilon_t^r(\omega) = 1 + 4\pi P_t(\omega)/E_t^{\mathrm{ext}}(\omega), \tag{5}$$

$$\varepsilon_\ell^r(\omega) = 1 + 4\pi P_\ell(\omega)/E_\ell^{\mathrm{ext}}(\omega), \tag{6}$$

where P_t (P_ℓ) and E_t^{ext} (E_ℓ^{ext}) are the induced polarization and the external field along the transverse (longitudinal) direction. The functions ε_t^r and ε_ℓ^r are related to the conventional dielectric function through[15]

$$\varepsilon_t^r = \varepsilon, \tag{7}$$

$$\varepsilon_\ell^r = 2 - 1/\varepsilon. \tag{8}$$

Using these relations, the IR absorption functions of Eqs. (1) and (2) have a simple expression in terms of ε_t^r and ε_ℓ^r,

$$I_t(\omega) = \frac{\omega d}{c}\mathrm{Im}\;\varepsilon_t^r(\omega), \tag{9}$$

$$I_\ell(\omega) = \frac{\omega d}{c}\mathrm{Im}\;\varepsilon_\ell^r(\omega). \tag{10}$$

The advantage of this formulation is that the determination of the longitudinal absorption function I_ℓ does not require the *explicit* inversion of the dielectric function. Equations (9) and (10) indicate that, in order to obtain the IR spectra of a thin film, we only need to compute the dielectric-response functions $\varepsilon_t^r(\omega)$ and $\varepsilon_\ell^r(\omega)$.

In the following we shall not discuss the computation of vibrational lifetimes due to anharmonic effects, electron-phonon interaction, or impurity scattering. In principle, the evaluation of the phonon lifetimes due to phonon-phonon scattering[18] or electron-phonon scattering[19] can be performed as a separate step.

1. Transverse-optical spectrum

In order to compute the transverse dielectric response ε_t^r required for the TO absorption spectrum, we observe that the external field E_t^{ext} coincides with the macroscopic self-consistent field E_t due to the electrostatic boundary conditions at the surface. Hence, the transverse dielectric function ε_t^r of the computational cell is given by the standard expression for the bulk dielectric permittivity,[20]

$$\varepsilon_t^r(\omega) = \varepsilon_{\alpha\alpha}^\infty - \frac{4\pi}{\Omega}\sum_n \frac{Z_{n,\alpha}^B Z_{n,\alpha}^B}{\omega^2 - \omega_{t,n}^2 - i\eta}, \tag{11}$$

where the mode-effective Born charge is defined as

$$Z_{n,\alpha}^B = \sum_I Z_{n,I\alpha}^B, \tag{12}$$

$$Z^B_{n,I\alpha} = \sum_\beta \frac{\xi^{t,n}_{I\beta}}{\sqrt{m_I}} Z^B_{I,\alpha\beta}. \tag{13}$$

In Eqs. (11)–(13), Ω is the volume of the supercell, m_I and $Z^B_{I,\alpha\beta}$ are the atomic mass and the Born dynamical charge tensor for the atom I, the index n runs over the vibrational modes, and the Greek subscripts refer to Cartesian directions. In Eq. (11), the index α needs to be taken along a transverse direction (we assume here a reference frame aligned with the surface). The vibrational frequencies $\omega_{t,n}$ and their corresponding normalized eigenmodes $\xi^{t,n}_{I\alpha}$ are obtained by diagonalizing the analytical part $C^{\alpha\beta}_{IJ}$ of the dynamical matrix.[20] By combining Eqs. (9) and (11), we obtain the transverse IR absorption function,

$$I_t(\omega) = \frac{2\pi^2}{Ac} \sum_n (Z^B_{n,\alpha})^2 \delta(\omega - \omega_{t,n}), \tag{14}$$

where A denotes the transverse area of the supercell.

2. Longitudinal-optical spectrum

In order to compute the longitudinal response ε^r_ℓ from Eq. (6), it is convenient to express the induced polarization in terms of the external field rather than the macroscopic self-consistent field E_ℓ: $P_\ell = P_\ell(E^{\text{ext}}_\ell)$. For this purpose, we first write the induced polarization along the longitudinal direction as a function of the self-consistent macroscopic field E_ℓ,[21]

$$P_\ell = \frac{1}{4\pi}(\varepsilon^\infty_{\alpha\alpha} - 1)E_\ell + \frac{1}{\Omega}\sum_{I\beta} Z^B_{I,\alpha\beta} u_{I\beta}(E_\ell), \tag{15}$$

where $u_{I\beta}(E_\ell)$ indicate the ionic displacements induced by the self-consistent field E_ℓ and α is taken along the longitudinal direction. Second, we write the dynamical equation for the harmonic motion of the ions,[21]

$$\omega^2 u_{I\beta}(\omega) = \sum_{J\gamma} C^{\beta\gamma}_{IJ} u_{J\gamma}(\omega) - Z^B_{I,\beta\alpha} E_\ell. \tag{16}$$

Third, we state the relation between the external field E^{ext}_ℓ and the macroscopic self-consistent field E_ℓ,

$$E^{\text{ext}}_\ell = E_\ell + 4\pi P_\ell, \tag{17}$$

which follows from the conservation of the longitudinal component of the displacement field across the surface of the film.

By combining Eqs. (15)–(17) we obtain

$$\omega^2 u_{I\beta}(\omega) = \sum_{J\gamma} C^{\beta\gamma}_{\ell,IJ} u_{J\gamma}(\omega) - Z^C_{I,\beta\alpha} E^{\text{ext}}_\ell, \tag{18}$$

which is formally similar to Eq. (16), except for the replacement of the Born charges with the corresponding *Callen* charges ($Z^C_{I,\beta\alpha} = Z^B_{I,\beta\alpha}/\varepsilon^\infty_{\alpha\alpha}$; see Ref. 20) and the matrix of force constants C with the *longitudinal* dynamical matrix C_ℓ defined as follows:

$$C^{\beta\gamma}_{\ell,IJ} = C^{\beta\gamma}_{IJ} + \frac{4\pi}{\Omega}\frac{1}{\varepsilon^\infty_{\alpha\alpha}} Z^B_{I,\beta\alpha} Z^B_{J,\alpha\gamma}. \tag{19}$$

The induced displacements can now be evaluated by inverting Eq. (18) through the diagonalization of the longitudinal dynamical matrix C_ℓ. By inserting the induced displacements in Eq. (15) and then using Eq. (6), we obtain the dielectric response to a longitudinal external field,

$$\varepsilon^r_\ell(\omega) = 2 - \frac{1}{\varepsilon^\infty_{\alpha\alpha}} - \frac{4\pi}{\Omega}\sum_n \frac{Z^C_{n,\alpha} Z^C_{n,\alpha}}{\omega^2 - \omega^2_{\ell,n} - i\eta}, \tag{20}$$

where the mode-effective Callen charges are given by

$$Z^C_{n,\alpha} = \sum_{I\beta} \frac{\xi^{\ell,n}_{I\beta}}{\sqrt{m_I}} Z^C_{I,\alpha\beta}. \tag{21}$$

In Eq. (21), the vibrational frequencies $\omega_{\ell,n}$ and their corresponding normalized eigenmodes $\xi^{\ell,n}_{I\alpha}$ correspond to the longitudinal dynamical matrix. We note that in the oscillator strengths of Eq. (20) we have the Callen charges as opposed to the Born charges of Eq. (11). Similarly to the case of the transverse absorption function, we now combine Eqs. (10) and (20) to obtain the longitudinal IR absorption function,

$$I_\ell(\omega) = \frac{2\pi^2}{Ac} \sum_n (Z^C_{n,\alpha})^2 \delta(\omega - \omega_{\ell,n}). \tag{22}$$

Equations (14) and (22) provide a scheme for calculating the IR absorption of a surface or a thin film. However, practical calculations are often performed within a supercell geometry, which will include the surface or thin film of interest, the substrate, and possibly some vacuum. Since the determination of the Born and Callen charges as well as the longitudinal dynamical matrix do depend on the *macroscopic* dielectric response of the combined system, it is important to understand how the IR absorption function will depend on the choice of the supercell. Section II C is devoted to clarifying this issue.

C. Local absorption spectra

In this section we repeat the derivation presented in Sec. II B by considering the IR absorption functions associated with specific atomic or molecular layers of a larger structure. This derivation is useful, for instance, to analyze the IR absorption of an interface with a complex chemical grading.[9] The derivation is based on the concept of a *local* dielectric permittivity introduced in Ref. 11. In analogy with Eqs. (5) and (6), the local dielectric responses will be expressed in terms of the external electric field. As in Ref. 11, the local dielectric functions (and the associated IR absorption functions) are intended to describe the response of atomistic layers with a thickness of ~2–3 Å. The key observation in the following derivation is that, while we start from the local dynamical charges $\zeta_{I,\alpha\beta}$ to correctly describe the local induced dipoles,[11] we end up with expressions involving only the Born or the Callen charges.

1. Transverse-optical spectrum

The local transverse dielectric response $\varepsilon_t^r(x;\omega)$ to the external electric field E_t^{ext} is written as follows [cf. Eqs. (3) and (4) of Ref. 11; x is taken along the longitudinal direction]:

$$\varepsilon_t^r(x;\omega) = 1 + 4\pi \frac{\bar{\bar{p}}_t(x;\omega)}{E_t^{\text{ext}}(\omega)}, \tag{23}$$

where $\bar{\bar{p}}_t(x;\omega)$ is the induced dipole density of an atomistic layer. The double bars indicate that the planar average along the transverse directions and a suitable smoothing along the longitudinal direction have been performed.[11] In analogy with Eq. (15), the induced dipole is obtained as follows:

$$\bar{\bar{p}}_t(x;\omega) = \frac{1}{4\pi}[\varepsilon_{\alpha\alpha}^{\infty}(x) - 1]\bar{\bar{e}}_t(x;\omega) + \frac{1}{A}\sum_{I\beta} \zeta_{I,\alpha\beta} u_{I\beta}(E_t) w(x - R_{I\alpha}), \tag{24}$$

with α along a transverse direction. In Eq. (24) the microscopic dipole is induced by the local transverse electric field $\bar{\bar{e}}_t(x;\omega)$, and the ionic contribution is taken into account via the local dynamical charges $\zeta_{I,\alpha\beta}$ introduced in Ref. 11. $R_{I\alpha}$ are the ionic coordinates and $w(x)$ is a spatial smoothing function localized around $x=0$. The extent of $w(x)$ has to be chosen consistently with the decay of the interatomic force constants.

In order to proceed, we make the following observations: (i) the local transverse electric field coincides with the external transverse field,

$$\bar{\bar{e}}_t(x;\omega) = E_t^{\text{ext}}(\omega), \tag{25}$$

(ii) the components of the effective charges and of the Born charges coincide along the transverse directions by construction [cf. the definition of local charges in Eq. (24) of Ref. 11], and (iii) the displacements appearing in Eq. (24) are obtained from the dynamical equation for the harmonic motion of the ions as in Sec. II B 1.[21] By combining Eqs. (23) and (24) and making use of these observations, we obtain the local transverse response function $\varepsilon_t^r(x;\omega)$,

$$\varepsilon_t^r(x;\omega) = \varepsilon_{\alpha\alpha}^{\infty}(x) - \frac{4\pi}{A}\sum_{In} \frac{Z_{n,I\alpha}^B Z_{n,I\alpha}^B}{\omega^2 - \omega_{t,n}^2 - i\eta} w(x - R_{I\alpha}). \tag{26}$$

The last equation allows us to write the density for the transverse IR absorption function $i_t(x,\omega) = \omega d \,\text{Im}\, \varepsilon_t^r(x;\omega)/c$ as

$$i_t(x,\omega) = \frac{2\pi^2}{Ac}\sum_{I,n} (Z_{n,I\alpha}^B)^2 \delta(\omega - \omega_{t,n}) w(x - R_{I\alpha}). \tag{27}$$

We note that the final expression does not involve the local dynamical charges or the local electric field but only the macroscopic Born charges.

2. Longitudinal-optical spectrum

The derivation of the local longitudinal dielectric response $\varepsilon_\ell^r(x;\omega)$ to an external electric field E_ℓ^{ext}, as well as of the associated local IR absorption function $i_\ell(x,\omega)$, proceeds in the same way as in Secs. II B 2 and II C 1. Therefore, we will not go through the derivation and only report the final expressions. The local longitudinal dielectric response is found to be

$$\varepsilon_\ell^r(x;\omega) = 2 - \frac{1}{\varepsilon_{\alpha\alpha}^{\infty}(x)} - \frac{4\pi}{A}\sum_{In} \frac{Z_{n,I\alpha}^C Z_{n,I\alpha}^C}{\omega^2 - \omega_{\ell,n}^2 - i\eta} w(x - R_{I\alpha}), \tag{28}$$

whereas the local density of the longitudinal absorption function is

$$i_\ell(x,\omega) = \frac{2\pi^2}{Ac}\sum_{I,n} (Z_{n,I\alpha}^C)^2 \delta(\omega - \omega_{\ell,n}) w(x - R_{I\alpha}). \tag{29}$$

At the end of this section on the formalism for calculating the IR absorption functions, it is interesting to note the remarkable symmetry between the expressions in Eqs. (14) and (22) as well as between their local decompositions [Eqs. (27) and (29)]. The only difference between TO and LO absorption corresponds to the use of the Born or Callen charges and to the transverse eigenmodes and eigenfrequencies or their longitudinal counterparts.

Another important observation is that the local absorption in Eqs. (27) and (29) involves again the Born and Callen charges, as opposed to the local dynamical charges.[9] From the point of view of practical calculations, this property implies that, in the case of an IR-active film (either interfacial layer or surface) on a transparent substrate, the total absorption calculated for the whole simulation cell corresponds to the absorption of the film. In other words, the IR absorption calculated through Eqs. (14) and (22) does not depend on the extent of vacuum or substrate included in the simulation cell.

This observation can be rephrased by stating that the IR absorption functions carry an additivity property and that the total absorption functions of a multilayer structure can be expressed as the sum of the corresponding functions of the individual layers. This additivity property is reflected in Eqs. (14) and (22), which only involve local quantities such as the *transverse* components of the Born charges and the *longitudinal* components of the Callen charges. Indeed, the transverse components of the Born charges can be calculated as the derivatives of the ionic forces with respect to the macroscopic transverse electric field, which is conserved across a layered structure. Therefore, the transverse components of the Born charges calculated for a bulk material and for the same material embedded in a layered structure do coincide (apart from the differences arising from the structural relaxation). A similar observation holds for the longitudinal components of the Callen charges. Indeed, these can be calculated as derivatives of the ionic forces with respect to the longitudinal displacement field, which is again conserved across a multilayer structure.

III. INFRARED ABSORPTION SPECTRA OF THE Si(100):H_2O SURFACE

A. Experimental background

1. Structure of the Si(100):H_2O *surface*

The adsorption of water on the Si(100) surface has been the subject of intensive experimental investigations. We here

limit ourselves to summarizing the findings which are relevant to the present study. A comprehensive review of the literature can be found in Ref. 22. The adsorption of water on the reconstructed Si(100)-(2×1) surface takes places through the dissociation of the H_2O molecule into OH hydroxyl groups and H species.[22] The main experimental evidence supporting this scenario derives from IR data indicating Si-H vibrational frequencies matching those of the monohydride species formed upon hydrogen adsorption on clean Si(100) surfaces. Similarly, the high frequency of the O-H stretching modes corresponds to that of the isolated hydroxyl group.[23–25] This model for water adsorption on Si(100)-(2×1) is further supported by photoemission and electron energy-loss experiments.[22] As a result of the dissociative chemisorption, the maximum water coverage on the clean Si(100) surface corresponds to 0.5 monolayer (ML) of Si, i.e., to the number of Si-Si dimers. The most likely path for dissociation involves the bonding of OH and H to the two Si atoms of the same dimer.[26] The adsorption of H and OH species on the Si-Si dimer lifts its characteristic buckling and leads to a Si-Si bond parallel to the surface.[27–29] Several studies indicate that the orientations of the dissociated species correspond to Si-H and Si-OH bonds contained within the plane defined by the surface normal and the Si-Si bond.[27–29] However, other works placed the O-H bond out of the latter plane and possibly pointing along the direction of the dimer row.[30,31] Some sensitivity of the O-H orientation to the temperature has also been observed,[26,32] and this could explain the different results reported by the various groups.

Scanning tunneling microscopy analysis revealed that the water-exposed Si(100) surface consists of both isolated hydroxyl groups and coupled hydroxyl groups chemisorbed on neighboring dimers and on the same side of the dimer row. No long-range order in the alignment of the OH groups has been reported.[10,33]

2. *Infrared data on the* $\mathbf{Si(100):H_2O}$ *surface*

Broadband Fourier-transform IR absorption spectra of the $Si(100):H_2O$ surface within an external transmission geometry have been presented in Ref. 10. The authors were able to cover a wide spectral range from the absorption of the Si-H bending vibrations around 600 cm^{-1} to the O-H stretching modes around 3650 cm^{-1}. The measurements were performed at 220 K, and at this temperature the water molecules were found to be completely dissociated. The IR spectra were recorded as a function of water coverage up to saturation. Most spectral features were observed to remain unchanged over the entire coverage range, suggesting that the structural configuration of the water layer did not change upon exposure of the Si(100) surface. In the spectral range corresponding to the O-H stretching vibrations three peaks were observed,[10] two close to each other and a third one lower in frequency by 20–30 cm^{-1}. Based on comparison with quantum-chemical cluster calculations of the vibrational frequencies, the authors proposed that two kinds of hydroxyl groups exist on the Si(100) surface: (i) isolated hydroxyl groups and (ii) coupled hydroxyl groups chemisorbed on the same end of two neighboring Si-Si dimers.

In a preceding work, the IR absorption spectra were recorded using a multiple internal reflection geometry[34] in the frequency range 2000–4000 cm^{-1}, covering the Si-H stretching vibrations around 2100 cm^{-1} and the O-H stretching modes.[25] Both *s*- and *p*-polarized spectra were reported for water dissociatively chemisorbed on the Si(100) surface at full coverage. For the Si-H bending modes a small blueshift of 2 cm^{-1} was observed from the *s*- to the *p*-polarized spectrum.

B. Computational setup

1. *Details of the calculations*

In order to calculate the IR absorption spectra of the $Si(100):H_2O$ surface we described the electronic structure using the local-density approximation to density-functional theory.[35] We described the valence electronic wave functions using a plane-wave basis set, and we accounted for the core-valence interaction using norm-conserving pseudopotentials[36] for Si atoms and ultrasoft pseudopotentials[37] for O atoms. We used plane-wave cutoffs of 24 and 200 Ry for the wave functions and the charge density, respectively.[38,39] We modeled the surface using a supercell containing 13 layers of a $2\sqrt{2}\times2\sqrt{2}$ Si slab. The slab exposes two (100) surfaces and periodic replicas are separated by 8 Å of vacuum. We sampled the Brillouin zone of the supercell at the Γ point. The matrix of the interatomic force constants was evaluated by taking numerical derivatives of the atomic forces for displacements of ±0.05 Å. Finite electric fields of ±0.05 V/Å were used to calculate the dynamical charges and the electronic permittivity.[40]

The accuracy in the calculation of the dynamical charges reflects the approximations used to describe the electronic structure and the dielectric response of the hydrated silicon surface. The use of the local-density approximation typically results in the overestimation of the dielectric polarization by about 10%.[41] Since the dynamical charges correspond to derivatives of the electronic polarization with respect to the ionic displacements, errors of similar magnitude should be expected for the charges. On the other hand, it has been shown that the dielectric polarization and the associated dynamical charge calculated through the use of the Γ-point formulation[40] of the Berry-phase theory generally approach their converged values from below.[42] Overall, it appears safe to assume that the infrared absorption intensities calculated here are accurate to within 10%.

For the calculation of the IR absorption spectra, we made the assumption that the external transmission geometry used in Ref. 10 can be approximately described using the expressions for the absorption of a freestanding film. In order to compare with the data reported in Ref. 25, we assumed that light is incident at an angle of 30° with respect to the surface normal.[34] The more involved expressions for the absorbance adopted in Ref. 25 are based on the assumption of a three-layer model and are not easily generalized to the present case where an atomistic description of the IR absorption is considered.

2. *Structural properties of the model surfaces*

To model the $Si(100):H_2O$ surface we assumed that the water molecules are fully dissociated into OH and H species

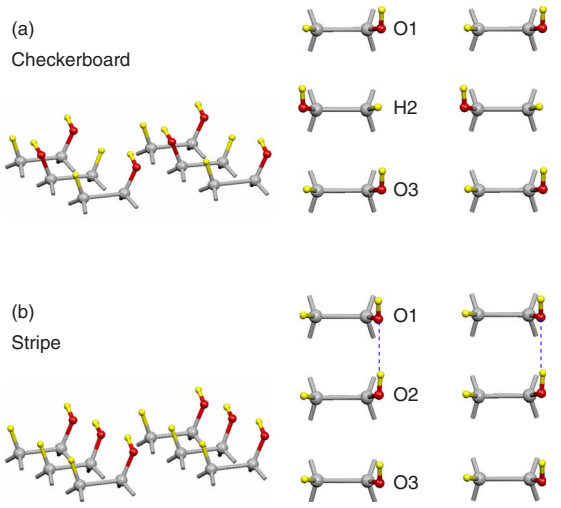

FIG. 1. (Color online) Ball-and-stick representation of the two structural models for the Si(100):H_2O surface considered in this work: (a) checkerboard phase and (b) stripe phase. The left (right) panels correspond to an oblique (top) view of the uppermost Si layer with the dissociated water molecules. Gray balls represent Si atoms, red (black) balls O atoms, and yellow (light gray) balls the H atoms. The dashed lines in (b) represent the hydrogen bonds. The structural parameters for the checkerboard model are as follows: d(Si-O)=1.64 Å, d(O-H)=0.97 Å, d(Si-H)=1.51 Å, ∠HOSi =118°, ∠HSiSi=109°, and ∠OSiSi=113°. The corresponding structural parameters for the stripe model are essentially the same (within 0.01 Å) except for the O-H bond length which in the stripe model is d(O-H)=1.00 Å.

bonded to the two Si atoms of the same dimer (cf. Sec. III A 1). We considered two structural configurations. In the first configuration, which we refer to as "stripe" phase hereafter, the hydroxyl groups of neighboring dimers are located on the same side of the dimer row. In the second configuration, named "checkerboard" phase in the following, the OH groups of neighboring dimers are located on the opposing sides of the row. The latter configuration is used to describe the case of OH groups and H species chemisorbed on isolated dimers. A ball-and-stick representation of these structural models is given in Fig. 1.

The relaxed Si-H, O-H, and Si-O bond lengths (cf. caption of Fig. 1) are close to those of silane [d(Si-H) =1.471 Å], molecular water [d(O-H)=0.957 Å], and silica [d(Si-O)=1.61 Å], respectively. The hydroxyl groups are found to be oriented almost parallel to the direction normal to the dimers (within 6°), in agreement with the experimental data in Refs. 30 and 31. The structural parameters obtained in the present work are in good agreement with those reported in a previous first-principles theoretical study based on cluster models of the hydrated Si(100) surface.[43]

In the checkerboard phase, the relaxed distances between the OH and H species attached to neighboring dimers on a row [Fig. 1(a)] are very similar: d(O1-H2)=3.72 Å and d(H2-O3)=3.84 Å. This indicates that the coupling between neighboring dimers on the same row is rather weak. On the other hand, in the stripe phase the O-O distances between neighboring dimers in the same row [Fig. 1(b)] are found to be d(O1-O2)=3.53 Å and d(O2-O3)=4.09 Å, indicating that the Si-O1 and Si-O2 bonds are canted toward each other. This behavior can be ascribed to the formation of hydrogen bonds between hydroxyl groups on the same side of the dimer row and corresponds to the formation of dimer pairs in the stripe phase. As a consequence of such interactions, the stripe phase is energetically favored over the checkerboard phase by 26 meV/H_2O (0.61 kcal/mol).

TABLE I. IR-active modes of the Si(100):H_2O surface: comparison between calculated and measured (Ref. 10) TO frequencies. The values between brackets represent the standard deviation for the group of vibrational modes of the same kind found around a given frequency. The frequency spread arises from the slightly nonsymmetric relaxation of the model surfaces. The symbols s and b refer to stretching and bending modes, respectively. The symbols "∥" and "⊥" in the Si-H bending modes indicate whether the H atoms move mostly parallel or perpendicular to the surface, respectively. Note the doublets in the stripe model, arising from the intrarow dimer coupling due to the hydrogen bond formed between neighboring hydroxyl groups.

	Frequency (cm^{-1})		
Mode	Checkerboard	Stripe	Expt.
Si-H $b\parallel$	562 (2)	560 (4)	606, 619, 630
Si-H $b\perp$	587 (2)	588 (4)	
O-H b	740 (8)	771 (8), 813 (8)	798, 823
Si-O s	889 (2)	867 (2), 897 (4)	890
Si-H s	2077 (3)	2090 (2)	2085
O-H s	3410 (3)	3346 (3), 3397 (1)	3655, 3675, 3683

While we here consider the Si(100):H_2O surface at full coverage (0.5 water ML), our model structures should be representative of configurations with low water coverage exhibiting the same structures of isolated and coupled dimers. In fact, in the checkerboard model the dimers do not interact appreciably along the row, while in the stripe model they interact in pairs. In addition, the negligible dependence of the IR spectra on water coverage (cf. Sec. III A 2) indicates that the structural and vibrational properties of the isolated and coupled dimers remain essentially unchanged upon water exposure.

C. Results

1. Frequencies of the infrared-active modes

In Table I, we compare the calculated transverse-optical frequencies of the IR-active modes of the Si(100):H_2O surface with the experimental data from Ref. 10. The Si-O and Si-H stretching modes are in good agreement with experiment, while for the Si-H and O-H bending modes our calculations underestimate the experimental data by 10–40 cm^{-1}. The frequencies of the O-H stretching are severely underestimated by our calculations (up to 9%, corresponding to about 300 cm^{-1}). The latter discrepancy can be ascribed to the use of an O pseudopotential with a relatively large core cutoff radius of 1.3 a.u., 50% larger than half the O-H bond length.

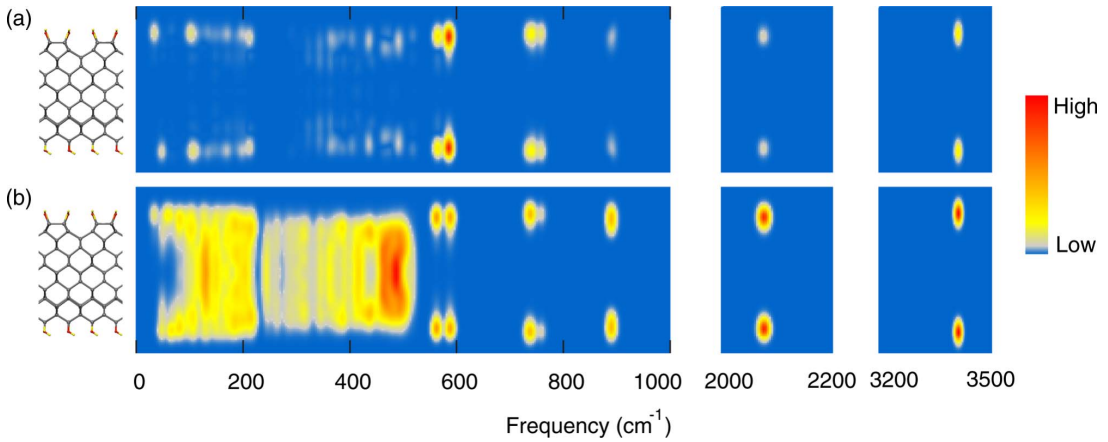

FIG. 2. (Color online) IR absorption corresponding to the checkerboard model of the $Si(100):H_2O$ surface, spatially resolved along the longitudinal coordinate (vertical axis). (a) Density of the IR absorption obtained from Eq. (27) by replacing the delta function in the frequency domain with a Lorentzian of width 5 cm^{-1} and the delta function in the longitudinal coordinate with a Gaussian of width 1 Å. (b) Local density of vibrational states for comparison. Arbitrary units are used for the density of IR absorption and for the density of vibrational states. The ball-and-stick models on the left indicate the spatial location of the absorption peaks across the slabs. In the frequency range 0–500 cm^{-1} the interior of the slab exhibits a significant density of states corresponding to the vibrational modes of bulk Si [panel (b)], which do not contribute to the IR absorption to first order in the electric-field strength [panel (a)].

As discussed in Sec. III A 2, the appearance of multiplets in the experimental spectra has been assigned to the presence of both isolated dimers (singlets) and intrarow coupled dimers (doublets). Our calculations confirm this assignment for the O-H and Si-O vibrational modes, although they do not support a similar assignment for the Si-H bending modes. Indeed, for the case of the Si-H bending vibrations, our calculations predict a doublet structure for both the checkerboard and the stripe models. This doublet arises from the anisotropic force constants associated with Si-H bending vibrations either within the plane defined by the Si-H bond and the dimer or outside of this plane. In particular, the calculated frequencies for the doublets of the stripe and the checkerboard models are essentially the same. This indicates that, in the stripe phase, intrarow coupling between the Si-H bonds does not take place; hence the corresponding triplet structure is not to be expected.

Gurevich *et al.*[10] identified two peaks in the frequency range corresponding to the O-H bending modes (~800 cm^{-1}). In the same frequency range our calculation reveals a triplet structure, raising the question on whether a third peak has been missed in the analysis of the experimental data. A careful inspection of Fig. 1(g) of Ref. 10 actually shows that the main peak at 823 cm^{-1} is accompanied by a smaller peak at 798 cm^{-1} (identified by the authors) and a mild shoulder at 840 cm^{-1}. We tentatively assign this shoulder to the highest vibrational frequency of the O-H bending modes of the intrarow coupled dimers. A similar assignment can be proposed for the Si-O stretching modes around 900 cm^{-1}, although the situation there is less clear since the IR intensity is comparable to the noise level.[10]

2. Spatially resolved absorption intensity

Figure 2 shows the density of the transverse infrared absorption obtained for the checkerboard model of the $Si(100):H_2O$ surface using Eq. (27). The results for the stripe model are qualitatively similar. The IR absorption takes place at the surfaces of the model slabs and becomes negligible within the Si substrate. This is consistent with the observation that the dynamical charges of bulk Si are vanishing due to inversion symmetry, making the slab interior transparent to IR radiation (to linear order). Close inspection of Fig. 2 reveals that the IR-active layers correspond to the water adsorbate and to a lesser extent to the outermost layer of Si atoms, i.e., the Si dimers. The vibrations of the adsorbate account for 78% of the total IR absorption, whereas the Si dimers contribute for 18%. The second, third, and fourth Si layers counting from the surface contribute for 2.2%, 1.9%, and 0.4% of the total absorption, respectively. The significant absorption taking place within the Si dimer rows relates to the local breaking of inversion symmetry for the Si atoms at the surface.

3. Intensities of the absorption peaks

Since the IR absorption takes place at the surfaces of the model slabs (cf. Sec. III C 2), it is appropriate to calculate the total absorption of each surface as half the total absorption of the periodic supercell, consisting of vacuum, silicon, and two surfaces. Since we did not include the lifetime broadening in our calculations, it is convenient to focus on the absorption strengths [corresponding to the magnitude of the peaks in Eqs. (14) and (22)], as opposed to the absorption functions. The extraction of the absorption strengths from experiment is performed by straightforwardly integrating the area underlying the measured peaks. This procedure is meaningful since the absorption peaks in the experimental spectra are well separated in energy (Fig. 2).

We give the calculated infrared absorption strengths for both the checkerboard and the stripe model structures in Fig. 3. The largest strengths are calculated for the Si-H bending modes in the TO spectra and for the O-H bending modes in both the TO and the LO spectra. The IR absorption associ-

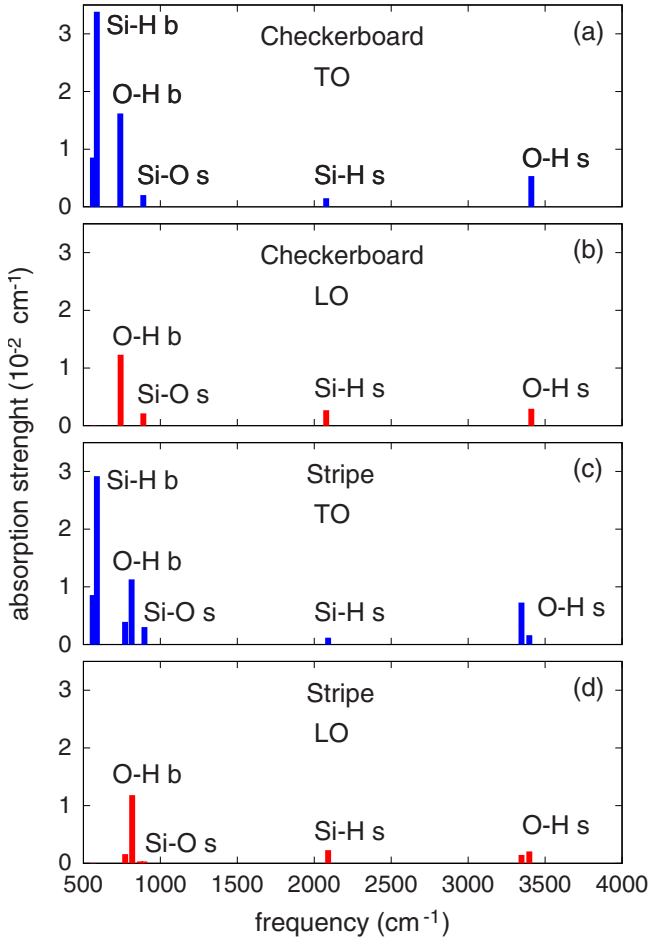

FIG. 3. (Color online) Infrared absorption strengths of the $Si(100):H_2O$ surface at full coverage: [(a) and (c)] strength of the transverse absorption function [from the strength of the peaks in Eq. (14)] and [(b) and (d)] strength of the longitudinal absorption function [from the strength of the peaks in Eq. (22)]. Panels (a) and (b) correspond to the checkerboard model, while (c) and (d) are for the stripe model. The characteristic vibrational modes involved are indicated. The symbols *s* and *b* indicate stretching and bending, respectively.

ated with the Si-H and the Si-O stretching vibrations is rather small in all cases. The Si-H bending motion absorbs only radiation polarized parallel to the surface because the bond is almost vertical (20° with respect to the normal direction). In the spectra for the stripe phase we see the appearance of doublets, associated with the dimer pairs formed on the surface as a consequence of the hydrogen bonds between neighboring hydroxyl groups (cf. Table I).

The comparison with the experimental data in Ref. 10 is presented in Table II. We study the case of *p*-polarized light incident at a grazing angle of 30° using Eq. (3).[34] The fraction of isolated and of uncoupled dimers in the experiment is unknown, therefore we consider three situations: (i) there are only isolated dimers on the surface (checkerboard phase), (ii) only coupled dimers (stripe phase), or (iii) there is a distribution of isolated and coupled dimers in equal amounts. Considering the higher thermodynamic stability of the stripe phase (cf. Sec. III B 2), the actual surface might correspond

TABLE II. Integrated IR absorption intensities for the $Si(100):H_2O$ surface at full coverage. We calculated the absorption corresponding to *p*-polarized radiation at grazing incidence (30°) for the checkerboard phase, the stripe phase, and a mixture containing equal amounts of isolated and coupled dimers (i.e., 50% stripe phase+50% checkerboard phase). The experimental data were obtained by integrating the area under the measured absorption peaks reported in Figs. 1(e), 1(g), and 1(h) of Ref. 10. The multiplet structures in both the theoretical and the experimental data were integrated together in order to obtain one single absorption strength for each family of IR-active modes.

	Absorption intensity (10^{-2} cm^{-1})			
Mode	Checkerboard	Stripe	50%+50%	Expt.
Si-H *b*	2.13	1.89	2.01	1.77
O-H *b*	2.66	2.77	2.71	1.71
Si-O *s*	0.43	0.26	0.35	0.43
Si-H *s*	0.48	0.40	0.44	0.44
O-H *s*	0.71	0.97	0.84	0.52

to a situation in between cases (ii) and (iii) above. We find that the calculations are in rather good agreement with experiment, apart from the O-H bending modes whose IR absorption is overestimated by 60% in our calculations. However, it is important to note that this comparison concerns absolute intensities and that the experimental strengths were obtained through direct integration of the measured spectra. The origin of the discrepancy for the O-H bending modes is unclear. It has previously been suggested that the O-H bending mode and the Si-O stretching mode may interact significantly due to their similar displacement patterns and vibrational frequencies and that the local-density approximation tends to overestimate such interaction as compared to more accurate quantum-chemical methods.[44] It is possible, at least in principle, that a better description of the coupling between O-H bending and Si-O stretching modes and the associated mode-effective charges could improve the comparison between our calculated absorption intensities and the experimental data.

As a last point, we compare the calculated LO-TO splitting with the experimental data in Ref. 25. Figure 1 of Ref. 25 reports the *s*- and *p*-polarized IR absorption spectra in the energy range corresponding to the Si-H stretching modes. The shift of the Si-H peak from *s*- to *p*-polarized light amounts to 2 cm^{-1} (from 2080 to 2082 cm^{-1}). Our calculations yield LO-TO splitting of ~0.1 cm^{-1} for the Si-H stretching modes (0.10 cm^{-1} in the stripe phase and 0.13 cm^{-1} in the checkerboard phase). Hence, both theory and experiment point to very small LO-TO splittings in the vibrations of the adsorbate layer at the $Si(100):H_2O$ surface.

IV. CONCLUSIONS

In this work we described in detail the formalism introduced in Ref. 11 to calculate the IR absorption at surfaces and interfaces from first-principles, and we presented an ap-

plication to the case of the hydrated Si(100) surface at full coverage. We were able to calculate both the transverse and the longitudinal components of the IR absorption and to spatially resolve the IR absorption intensity across the surface. Our results compare favorably with experiment and allow us to revise previous assignments of the experimental spectra in light of our atomistic description of the $Si(100):H_2O$ surface.

In order to make comparison with experiment we have focused on the absorption strengths (i.e., the integrated absorption signals). A more comprehensive comparison taking into account the spectral broadening would require the calculation of the vibrational lifetimes arising from anharmonic effects as well as the effect of structural and chemical inhomogeneities at the surface. The calculation of the lifetime broadening due to phonon-phonon scattering has been demonstrated for bulk semiconductors[18] and is in principle possible in the present situation. However, this calculation would require the evaluation of third order derivatives of the total energy with respect to the atomic displacements, which is computationally demanding. On the other hand, the broadening of the spectral lines arising from structural inhomogeneities could be addressed by sampling a larger number of chemisorption configurations. While in the present work we have not explored these possibilities, we hope that our investigation will stimulate further efforts in these directions.

It is tempting to envision the use of our technique to study the composition and phase diagram of the $Si(100):H_2O$ surface through a combination of experimental data and theoretical analysis. Indeed it should be possible, at least in principle, to optimize the composition of the model surface in terms of isolated and coupled dimers in order to optimally fit the experimental spectra. This analysis might provide some useful insight into the composition of the hydrated Si(100) surface, which is still an open issue nowadays.

Such a combination of first-principles modeling and semiempirical fitting of the experimental data may generally open possibilities in the study of the structure and dynamics of adsorbates on surfaces. In particular, since IR spectra can be recorded *in situ* and in real time, this combination of experiment and theory may also prove useful for quantitative studies of chemical reactions.

Finally, we note that the calculations reported here rely on the concept of atomic-scale dielectric permittivity introduced in Ref. 11. The relation between this layer-resolved permittivity and the fully nonlocal dielectric function has been formally developed in the present work. The derivation provided here should help addressing the question on the range of applicability of the notion of local permittivity. Understanding the limits of validity of this description is particularly important nowadays, insofar a growing number of investigations of the dielectric response of nanoscale systems[45–49] have began to adopt the local permittivity concept.

ACKNOWLEDGMENTS

The calculations were performed at the central computational facilities of the Ecole Polytechnique Fédérale de Lausanne (EPFL) and at Swiss Center for Scientific Computing (CSCS).

APPENDIX A: RELATION WITH THE THEORY OF THE LOCAL PERMITTIVITY

We here establish the relation between the local permittivity $\varepsilon_{\alpha\beta}(x,\omega)$ introduced in Ref. 11 and the local dielectric response to an external field $\varepsilon^r_\ell(x,\omega)$ of Eq. (28). By taking α along the longitudinal direction, it can be shown that[15]

$$\varepsilon_{\alpha\alpha}(x,\omega)=[2-\varepsilon^{\mathrm{r}}_\ell(x,\omega)]^{-1}. \tag{A1}$$

For simplicity we only provide here an explicit expression for $\varepsilon^0_{\alpha\alpha}(x)=\varepsilon_{\alpha\alpha}(x,\omega=0)$ obtained by combining Eq. (A1) with Eq. (28),

$$[\varepsilon^0_{\alpha\alpha}(x)]^{-1}=[\varepsilon^\infty_{\alpha\alpha}(x)]^{-1}-\frac{4\pi}{A}\sum_{In}\frac{Z^C_{n,I\alpha}Z^C_{n,I\alpha}}{\omega^2_{\ell,n}}w(x-R_{I\alpha}). \tag{A2}$$

The last equation allows us to decompose the dielectric screening of a layered structure in terms of its atomic-layer contributions. With respect to methods based on the application of finite electric fields,[11] the formulation given by Eq. (A2) relies on a linear-response approach and provides more detailed information on the microscopic nature of the dielectric screening in the system. The two methods do provide the same profile for the atomic-scale dielectric permittivity.[50] The formulation presented in this section may prove helpful, for instance, to clarify the atomistic origin of the dielectric dead layer in nanoscale capacitors.[45]

APPENDIX B: RELATION BETWEEN THE LOCAL PERMITTIVITY AND THE NONLOCAL DIELECTRIC MATRIX

In Sec. II C, we made use of the concept of local dielectric permittivity introduced heuristically in Ref. 11. In this section we provide the relation between this local permittivity and the nonlocal dielectric matrix[51] $\varepsilon_{\alpha\beta}(\mathbf{r},\mathbf{r}')$ (where $\mathbf{r}$ and $\mathbf{r}'$ are the position vectors, and we omit the frequency dependence for ease of notation). We start by considering the relation between the microscopic induced polarization $p_\alpha(\mathbf{r})$ and the microscopic self-consistent electric field $e_\alpha(\mathbf{r})$,

$$p_\alpha(\mathbf{r})=\int d\mathbf{r}'\chi_{\alpha\beta}(\mathbf{r},\mathbf{r}')e_\beta(\mathbf{r}'), \tag{B1}$$

where $\chi_{\alpha\beta}(\mathbf{r},\mathbf{r}')$ is the nonlocal susceptibility, and the sum over repeated indices is understood. In Eq. (3) of Ref. 11 the local susceptibility $\chi^{\mathrm{loc}}_{\alpha\beta}(\mathbf{r})$ was introduced as follows:

$$\int d\mathbf{r}'w(\mathbf{r},\mathbf{r}')p_\alpha(\mathbf{r}')=\chi^{\mathrm{loc}}_{\alpha\beta}(\mathbf{r})\int d\mathbf{r}'w(\mathbf{r},\mathbf{r}')e_\beta(\mathbf{r}'). \tag{B2}$$

At variance with Eq. (3) of Ref. 11, Eq. (B2) explicitly shows the smoothing procedure applied to the microscopic induced dipole and to the microscopic self-consistent field through the smearing function $w(\mathbf{r},\mathbf{r}')$. In order to establish

the relation between $\chi^{\mathrm{loc}}_{\alpha\beta}(\mathbf{r})$ and $\chi_{\alpha\beta}(\mathbf{r},\mathbf{r}')$, we first apply the smoothing procedure to both sides of Eq. (B1),

$$\int d\mathbf{r}' w(\mathbf{r},\mathbf{r}') p_\alpha(\mathbf{r}') = \int d\mathbf{r}' \int d\mathbf{r}'' w(\mathbf{r},\mathbf{r}') \chi_{\alpha\beta}(\mathbf{r}',\mathbf{r}'') e_\beta(\mathbf{r}''). \tag{B3}$$

Second, we combine Eqs. (B2) and (B3) to obtain

$$\chi^{\mathrm{loc}}_{\alpha\beta}(\mathbf{r}) \int d\mathbf{r}' w(\mathbf{r},\mathbf{r}') e_\beta(\mathbf{r}') = \int d\mathbf{r}' \int d\mathbf{r}'' w(\mathbf{r},\mathbf{r}') \chi_{\alpha\beta}(\mathbf{r}',\mathbf{r}'') e_\beta(\mathbf{r}''). \tag{B4}$$

Now we introduce the dielectric permittivity tensors,

$$\varepsilon^{\mathrm{loc}}_{\alpha\beta}(\mathbf{r}) = \delta_{\alpha\beta} + 4\pi\chi^{\mathrm{loc}}_{\alpha\beta}(\mathbf{r}) \tag{B5}$$

and

$$\varepsilon_{\alpha\beta}(\mathbf{r},\mathbf{r}') = \delta_{\alpha\beta}\delta(\mathbf{r},\mathbf{r}') + 4\pi\chi_{\alpha\beta}(\mathbf{r},\mathbf{r}'), \tag{B6}$$

with $\delta_{\alpha\beta}$ and $\delta(\mathbf{r},\mathbf{r}')$ being the Kronecker and Dirac deltas, respectively. The inverse of the nonlocal dielectric matrix provides the relation between the self-consistent microscopic field $e_\alpha(\mathbf{r})$ and the external electric field $E^{\mathrm{ext}}_\alpha(\mathbf{r})$,

$$e_\alpha(\mathbf{r}) = \int d\mathbf{r}' \varepsilon^{-1}_{\alpha\beta}(\mathbf{r},\mathbf{r}') E^{\mathrm{ext}}_\beta(\mathbf{r}'). \tag{B7}$$

By combining Eqs. (B4)–(B7) we obtain

$$\int d\mathbf{r}' w(\mathbf{r},\mathbf{r}') E^{\mathrm{ext}}_\alpha(\mathbf{r}') = \varepsilon^{\mathrm{loc}}_{\alpha\beta}(\mathbf{r}) \int d\mathbf{r}' \int d\mathbf{r}'' w(\mathbf{r},\mathbf{r}') \varepsilon^{-1}_{\beta\gamma}(\mathbf{r}',\mathbf{r}'') E^{\mathrm{ext}}_\gamma(\mathbf{r}''). \tag{B8}$$

We now take the external field uniform and oriented along the direction perpendicular to the film surface (which we assume to be $\alpha=3$ without loss of generality). The choice of a uniform external field is appropriate whenever the thickness of the film is much smaller than the wavelength of the field. This limit is well verified in the case of the IR absorption of surface adsorbates considered in the present work. Under these conditions, the diagonal component of the inverse local dielectric matrix $\varepsilon^{-1,\mathrm{loc}}_{33}(\mathbf{r})$ reads

$$\varepsilon^{-1,\mathrm{loc}}_{33}(\mathbf{r}) = \int d\mathbf{r}' w(\mathbf{r},\mathbf{r}') \int d\mathbf{r}'' \varepsilon^{-1}_{33}(\mathbf{r}',\mathbf{r}'+\mathbf{r}''). \tag{B9}$$

Let us denote by λ being the localization length of the inverse nonlocal dielectric matrix.[11] If the smoothing kernel $w(\mathbf{r},\mathbf{r}')$ is chosen to be unity for $|\mathbf{r}-\mathbf{r}'|<\lambda$ and vanishing for $|\mathbf{r}-\mathbf{r}'|>\lambda$, then the integration over $\mathbf{r}''$ in Eq. (B9) can be replaced by

$$\int d\mathbf{r}'' \varepsilon^{-1}_{33}(\mathbf{r}',\mathbf{r}'+\mathbf{r}'') \simeq \int d\mathbf{r}'' w(\mathbf{r}',\mathbf{r}'') \varepsilon^{-1}_{33}(\mathbf{r}',\mathbf{r}'+\mathbf{r}''). \tag{B10}$$

Under these conditions, Eq. (B9) can be rewritten as

$$\varepsilon^{-1,\mathrm{loc}}_{33}(\mathbf{r}) = \int d\mathbf{r}' \int d\mathbf{r}'' w(\mathbf{r},\mathbf{r}') w(\mathbf{r}',\mathbf{r}'') \varepsilon^{-1}_{33}(\mathbf{r}',\mathbf{r}'+\mathbf{r}''), \tag{B11}$$

providing a transparent relation between the local permittivity introduced in Ref. 11 and the nonlocal dielectric matrix. Whenever the principal axes of the dielectric tensor are aligned with the surface of the film, the off-diagonal components of the dielectric matrices vanish and the inversion of Eq. (B11) becomes straightforward.

[1] J. M. Buriak, Chem. Rev. (Washington, D.C.) **102**, 1271 (2002).
[2] G. Cicero and A. Catellani, J. Chem. Phys. **122**, 214716 (2005).
[3] G. Cicero, A. Catellani, and G. Galli, Phys. Rev. Lett. **93**, 016102 (2004).
[4] D. Prendergast, J. C. Grossman, A. J. Williamson, J.-L. Fattebert, and G. Galli, J. Am. Chem. Soc. **126**, 13827 (2004).
[5] Y. J. Chabal, Surf. Sci. Rep. **8**, 211 (1988).
[6] Y. J. Chabal and K. Raghavachari, Phys. Rev. Lett. **53**, 282 (1984).
[7] M. K. Weldon, B. B. Stefanov, K. Raghavachari, and Y. J. Chabal, Phys. Rev. Lett. **79**, 2851 (1997).
[8] B. B. Stefanov, A. B. Gurevich, M. K. Weldon, K. Raghavachari, and Y. J. Chabal, Phys. Rev. Lett. **81**, 3908 (1998).
[9] F. Giustino and A. Pasquarello, Phys. Rev. Lett. **95**, 187402 (2005).
[10] A. B. Gurevich, B. B. Stefanov, M. K. Weldon, Y. J. Chabal, and K. Raghavachari, Phys. Rev. B **58**, R13434 (1998).
[11] F. Giustino and A. Pasquarello, Phys. Rev. B **71**, 144104 (2005).
[12] L. L. Hirst, Rev. Mod. Phys. **69**, 607 (1997).
[13] K. Huang, Proc. R. Soc. London **A208**, 352 (1951).
[14] D. W. Berreman, Phys. Rev. **130**, 2193 (1963).
[15] C. T. Kirk, Phys. Rev. B **38**, 1255 (1988).
[16] R. Ruppin and R. Englman, Rep. Prog. Phys. **33**, 149 (1970).
[17] E. Burstein, S. Iwasa, and Y. Sawada, Proceedings of the E. Fermi International School of Physics, Course XXXIV, Optical Properties of Solids, Varenna, 1965, edited by J. Tauc (Academic, New York, 1966), p. 431.
[18] A. Debernardi, Phys. Rev. B **57**, 12847 (1998).
[19] R. Bauer, A. Schmid, P. Pavone, and D. Strauch, Phys. Rev. B **57**, 11276 (1998).
[20] X. Gonze and C. Lee, Phys. Rev. B **55**, 10355 (1997).
[21] W. Cochran and R. A. Cowley, J. Phys. Chem. Solids **23**, 447 (1962).
[22] M. A. Henderson, Surf. Sci. Rep. **46**, 1 (2002).

[23] Y. J. Chabal, J. Vac. Sci. Technol. A **3**, 1448 (1985).
[24] Y. J. Chabal and S. B. Christman, Phys. Rev. B **29**, 6974 (1984).
[25] Y. J. Chabal, Phys. Rev. B **29**, 3677 (1984).
[26] A. L. Johnson, M. M. Walczak, and T. E. Madey, Langmuir **4**, 277 (1988).
[27] N. Franco, J. Chrost, J. Avila, M. C. Asensio, C. Muller, E. Dudzik, A. J. Patchett, I. T. McGovern, T. Giebel, R. Lindsey, V. Fritzsche, A. M. Bradshaw, and D. P. Woodruff, Appl. Surf. Sci. **123–124**, 219 (1998).
[28] M. Nishijima, K. Edamoto, Y. Kubota, S. Tanaka, and M. Onchi, J. Chem. Phys. **84**, 6458 (1986).
[29] L. Andersohn and U. Kohler, Surf. Sci. **284**, 77 (1993).
[30] R. McGrath, R. Cimino, W. Braun, G. Thornton, and I. T. McGovern, Vacuum **38**, 251 (1988).
[31] K. Fives, R. McGrath, C. Stephens, I. T. McGovern, R. Cimino, D. S. L. Law, A. L. Johnson, and G. Thornton, J. Phys.: Condens. Matter **1**, SB105 (1989).
[32] C. U. S. Larsson, A. L. Johnson, A. Flodstrom, and T. E. Madey, J. Vac. Sci. Technol. A **5**, 842 (1987).
[33] M. Chander, Y. Z. Li, J. C. Patrin, and J. H. Weaver, Phys. Rev. B **48**, 2493 (1993).
[34] Y. J. Chabal, E. E. Chaban, and S. B. Christman, J. Electron Spectrosc. Relat. Phenom. **29**, 35 (1983).
[35] J. P. Perdew and A. Zunger, Phys. Rev. B **23**, 5048 (1981).
[36] G. B. Bachelet, D. R. Hamann, and M. Schlüter, Phys. Rev. B **26**, 4199 (1982).
[37] D. Vanderbilt, Phys. Rev. B **41**, 7892 (1990).
[38] A. Pasquarello, K. Laasonen, R. Car, C. Lee, and D. Vanderbilt, Phys. Rev. Lett. **69**, 1982 (1992).
[39] K. Laasonen, A. Pasquarello, R. Car, C. Lee, and D. Vanderbilt, Phys. Rev. B **47**, 10142 (1993).
[40] P. Umari and A. Pasquarello, Phys. Rev. Lett. **89**, 157602 (2002).
[41] A. Dal Corso, S. Baroni, and R. Resta, Phys. Rev. B **49**, 5323 (1994).
[42] P. Umari and A. Pasquarello, Phys. Rev. B **68**, 085114 (2003).
[43] S. Carniato, J.-J. Gallet, F. Rochet, G. Dufour, F. Bournel, S. Rangan, A. Verdini, and L. Floreano, Phys. Rev. B **76**, 085321 (2007).
[44] K. Raghavachari, Y. J. Chabal, and L. M. Struck, Chem. Phys. Lett. **252**, 230 (1996).
[45] M. Stengel and N. Spalding, Nature (London) **443**, 679 (2006).
[46] F. Giustino and A. Pasquarello, Appl. Phys. Lett. **86**, 192901 (2005).
[47] N. Shi and R. Ramprasad, Appl. Phys. Lett. **91**, 242906 (2007).
[48] S. Wakui, J. Nakamura, and A. Natori, Jpn. J. Appl. Phys. **46**, 3261 (2007).
[49] B. Lee, C.-K. Lee, S. Han, J. Lee, and C. S. Hwang, J. Appl. Phys. **103**, 024106 (2008).
[50] F. Giustino, Ph.D. thesis, Ecole Polytechnique Fédérale de Lausanne, 2005.
[51] O. V. Dolgov and E. G. Maksimov, in *The Dielectric Function of Condensed Systems*, edited by L. V. Keldysh, D. A. Kirzhnitz, and A. A. Maradudin (North-Holland, Amsterdam, 1989), Secs. 2.1 and 4.1.